A Preliminary Study on the Mechanism of Early Lesions in the Subchondral Bone of a Rat Model of Intevertebral Disc Degeneration

HAO QU[1], FENG WANG[3], ZHIGANG LI[1], DAN WANG[4], FENG XU[2], HUI KANG[2], WEI HUANG[4], HENG WU[1], FAN WU[1] AND XIANHUA CAI[2*]

College of Acupuncture and Orthopedics, Hubei University of Chinese Medicine, [1]Department of Orthopedics, Hubei Provincial Hospital of Integrated Chinese and Western Medicine, [2]Department of Orthopedics Surgery, General Hospital of Central Theater Command, Wuhan, Hubei 430000, [3]Department of Orthopedics, Characteristic Medical Center of the Chinese People's Armed Police Force, [4]Department of Spine Surgery, Jinmen NO. 2 People's Hospital, Jingmen, Hubei 448000, China

Qu *et al.*: Mechanism of Early Lesions in the Subchondral Bone

To observe the lesion characteristics of vertebral subchondral bone by establishing a rat model of intervertebral disc degeneration. Thirty-two Sprague–Dawley rats were randomly divided into four groups of eight rats each, and one group served as the control group without any treatment. The rats in the experimental group were injected with 30 µl of anhydrous alcohol under the endplate (sub-endplate) above the Co6 vertebrae and 30 µl of phosphate buffered saline buffer under the endplate above the Co8 vertebrae. Eight rats were randomly taken for follow-up testing at 2, 4, and 8 w after establishment of models. The rats underwent imaging X-rays and magnetic resonance imaging to assess vertebral subchondral bone and intervertebral disc degeneration grades; then serum enzyme-linked immunosorbent assay was performed to measure tumor necrosis factor-alpha, interleukin-1 beta, type I procollagen amino-terminal peptide, type I collagen carboxy-terminal peptide, vascular endothelial growth factor A and endostatin. The Co5/Co6 and Co7/Co8 motion segments (including the adjacent vertebrae and intervertebral disc) were used to perform micro-computed tomography, histological staining with hematoxylin and eosin, sapphire green, and toluidine blue, as well as for detecting the expression of collagen type II, and vascular endothelial growth factor A expression. Collagen type II, aggregated proteoglycan (aggrecan), sox-9, vascular endothelial growth factor A by immunohistochemical tests. Imaging, histologic staining and immunohistochemistry confirmed the successful establishment of intervertebral disc degeneration model. Histological observations and immunohistochemical analysis showed progressive degeneration of major intervertebral disc structures. Blocking the intervertebral disc trophic pathway in the vertebral subchondral bone region can successfully establish intervertebral disc degeneration rat model, and the possible main lesion characteristics of the vertebral subchondral bone during this process include abnormal bone remodeling, destruction of blood vessels and enhanced inflammatory response.

Key words: Intervertebral disc degeneration, vertebral subchondral bone, model, animal, rat

Disc Degenerative Diseases (DDDs) have an increasingly negative impact on human health and the economy, and although they have been studied intensively, their specific mechanisms have not yet been fully understood. Vertebral Subchondral Bone (VSB) (also known as bony endplate) is thought to be deeply involved in the complex process of Integrated Dual Degree (IDD). As the most important trophic pathway of Intervertebral Disc (IVD), the IVD trophic disorder caused by its lesion may be the initiating factor of IDD.

However, since previous studies on experimental models of IDD have mainly focused on Nucleus Pulposus (NP) and Annulus Fibrosus (AF), there have been few studies on animal models that disrupt the nutrient pathway in the VSB region,

*Address for correspondence
E-mail: 19947615161@163.com

thereby inducing IDD; and the characteristics of VSB lesions in the course of IDD have not been fully elucidated. In this article, we describe the successful fabrication and validation of an IDD model by disrupting the nutrient pathway in the VSB region of SD rats, and more comprehensively document the characteristics of VSB lesions in the early stage of IDD, which will provide a possible reference for subsequent related studies.

MATERIALS AND METHODS

Ethical approval:

All operations performed on animal involving in this study were conducted in accordance with the guidelines for ethical review of laboratory animal welfare of the People's Republic of China (GB/T 35892-2018) and the guiding opinions on the kind treatment of laboratory animals issued by the Ministry of Science and Technology, and approved by the Ethics Committee of Hubei University of Traditional Chinese Medicine (No. HUCMS202204002).

Experimental animals, main materials and instruments:

Specific Pathogen-Free (SPF) grade 3 mo old male Sprague-Dawley (SD) rats were purchased from the Animal Experiment Center of Hubei University of Traditional Chinese Medicine [Animal License No: syxk(E)2017-0067], with a body mass of (455±12) g (mean±standard deviation). They were acclimatized and fed for 1 w, and were included in the experiment after they were healthy, had no deformity or injury in tail appearance, and had mature bone development and no obvious deformity by X-ray examination. Medical anhydrous ethanol (No. 1009218, Sinopharm Chemical Reagent Co., Ltd., China), sodium pentobarbital (Hangzhou Famcor Chemical Products Co., Ltd., China), optical microscope (NIKON ECLIPSE TI-SR, Japan), digital computerized imaging X-ray machine and 3.0 T medical superconducting magnetic resonance scanner (SIEMENS, Germany), micro-Computed Tomography (microCT) scanner (SCANCO, Switzerland), and a 3.0 T medical superconducting magnetic resonance scanner (SIEMENS, Germany) were used for the study.

Establishment of animal model:

Using the random grouping method, 32 SD rats were randomly divided into 4 groups of 8 rats each, with one group as the control group without any treatment. The other 3 groups of rats were used as experimental groups, and underwent subfloor puncture modeling, and 8 rats were randomly taken at 2, 4, and 8 w after the modeling to perform relevant tests, respectively. The specific operation of the rats was reported by Yuan et al.[1], with slight adjustments; after successful anesthesia, the rats were placed in the prone position, with the head tilted to one side, and kept warm by sterile cotton pads on the abdominal and dorsal sides. The skin of the rat's tail was sterilized with povidone-iodine three times, and after confirming that the rat's tail was parallel to the longitudinal axis of the trunk, a sterile sheet was spread. Under X-ray fluoroscopic guidance, Co5/Co6 and Co7/Co8 segments were localized, and a millimeter ruler was used to measure and mark the skin at the level of 3 mm distal to the IVD of the two segments and to measure the radius of the rat tail at that level. A length equal to the radius of the rat's tail was marked at the tip of the 9-gauge puncture needle. The needle is inserted vertically at the dorsal skin marking point of the rat's tail, and the depth of the needle is equal to the radius of the rat's tail at that level, i.e., the marking on the needle is just in contact with the skin of the rats tail. After positive lateral fluoroscopy to ensure that the puncture needle was near the center of the endplates of Co6 and Co8, the core of the puncture needle was withdrawn, and 30 µl of anhydrous ethanol was slowly injected into the center of the vertebral body near the endplates of Co6 through the heparin cap connected to the 50 µl micro feeder to ensure that the drug was well dispersed and there was no leakage. The heparin cap was carefully removed, and the puncture needle was removed after insertion of the needle core; the puncture point was immediately pressurized with a sterile cotton ball to ensure that there was no leakage, and then the puncture point was sterilized again. In the same method, 30 µl of Phosphate-Buffered Saline (PBS) solution was injected under the Co8 upper end plate as a control. After complete awakening from anesthesia, diet and activity were not restricted.

Assessment of imaging:

AMeasurement of Disc Height Index Percentage (DHI %) by X-ray: At 2, 4, and 8 w postoperatively, randomly selected rats were examined by X-ray

after anesthesia to assess the height of the intervertebral space and the morphology of the endplates. The X-ray equipment was used under photographic conditions; 50 mA, 50 kV. The calculation of DHI % was performed according to the method described by Kim *et al.*[2] and Han *et al.*[3]. Briefly, 3 parallel straight lines dividing the width of the IVD into 4 equal parts were made, and the ends of the lines intersected with the endplates on the other side of the adjacent vertebrae. The DHI was equal to the length of the 3 straight lines within the IVD added together multiplied by 2, and divided by the length of the 3 straight lines within the vertebrae on both sides of the 6 segments of the vertebral body. DHI %=(Postoperative DHI/preoperative DHI)×100 %

IDD degree grading were detected by Magnetic Resonance Imaging (MRI): MRI of the rat caudal spine was performed under anesthesia at preoperative and postoperative time points of 2, 4, and 8 w, respectively[3]. Senior imaging physicians took the form of blinded reading of the films, and graded the rat caudal spine IVDs according to the Pfirrmann grading through the median sagittal images[4].

Assessment of subchondral bone related parameters by microCT: At the preoperative and 2 w and 8 w postoperative time points, rats were randomly selected, and after death by overdose anesthesia, the Co5/Co6 and Co7/Co8 motion segments (including the adjacent vertebrae of each segment) of the rats were removed intact, and then immersed and fixed in a 10 % neutral formaldehyde solution for 48 h, and then microCT examination was performed to collect the relevant data including the relevant parameters of the subchondral bone plates of the adjacent endplates of the various IVDs; the thickness of cortical plate (Ct.), Thickness of Cortical plate (Ct.Th), Bone Mineral Density of Cortical plate (Ct. BMD); and parameters related to subchondral cancellous bone: Tb.BV/TV, Bone mineral density of trabecular bone, Tb.BV/TV, Bone mineral density of trabecular bone, Tb.BV/TV, Tb.BV/TV, Tb.BV/TV, Tb.BV/TV, Tb.BV/TV, Tb.BV/TV, Bb.BV/TV, Bb.BMD, Bb. BV/TV, bone mineral density of trabecular bone, Tb. BMD), Tb. Th, Tb. N *vs*. Tb.Sp. Comparison of the two segments at each time point to see if there was a statistically significant difference in each parameter.

Reliability analysis of data measurements: In order to assess the intra and inter-observer consistency of the relevant data, we re-measured the data from radiographs, MRI and microCT. Relevant data were measured independently by two senior orthopedic surgeons performing a blinded method. The same intra-observer sample was re-measured by the same observer after 1 mo. The intra-observer and inter-observer errors and coefficients of variation were calculated with reference to the method of Han *et al.*[3] to understand the magnitude of intra-observer errors.

The within-subject standard deviation (S_w) was calculated as follows:

$$S_w = \sqrt{\sum (x_1 - x_2)^2 / 2n}$$

The Percentage Coefficient of Variation (% CV) was calculated as follows:

$$\% \, CV = S_w / \sum (x_1 - x_2)^2 / 2n \times 100$$

Where, x_1 and x_2 are two measurements from the same sample. Inter-observer error was understood by analyzing measurement differences across observers; intra-observer error was understood by analyzing two measurements taken by the same observer 1 mo apart.

IDD histologic scoring:

At preoperative and postoperative time points of 2, 4, and 8 w, the above specimens were decalcified, routinely embedded, and made into wax blocks sequentially after completion of microCT examination. Hematoxylin and Eosin (HE) staining, toluidine blue staining and senna solid green staining were performed. And the pathological changes of each component of IVD tissues (including subchondral bone) were observed under multi-purpose microscope, and the samples were scored with IDD histological grade according to the IDD scoring scale (Table 1) reported by Allon *et al.*[5] (fig. 1).

Immunohistochemical analysis:

The expression of Collagen Type II (Col II) protein, aggregated proteoglycan (aggrecan), sox-9, Vascular Endothelial Growth Factor A (VEGFA), and CD31 was detected in the IVD, cartilage endplates, and bony endplates of the samples, which were used as reference markers for IDD and VSB lesions. Immunohistochemical (IHC) staining was performed using the following primary antibodies;

rabbit polyclonal sox-9 antibody (1:150 dilution; AF6330) (Affinity, UK), and rabbit polyclonal col II antibody (1:400 dilution; 28459-1-AP; Sanying, China); the staining was performed under an IX51 microscope (Olympus, Tokyo, Japan) for the preparation of staining.

Serologic markers testing:

At the preoperative and postoperative week 8 time points, 1 ml of blood was collected from the heart of each group of rats with a syringe, placed in a 1.5 ml centrifuge tube (without anticoagulant), and left to stand for 30 min at room temperature, then centrifuged for 10 min at 1500 ×g at room temperature, and then the upper layer of the serum was extracted, and the contents of the relevant indexes were measured by Enzyme-Linked Immunosorbent Assay (ELISA), Tumor Necrosis Factor-Alpha (TNF-α), Interleukin-1 Beta (IL-1β), type I Procollagen Amino Peptides (PAPPs), and sera were collected from the heart of rats of each group. The levels of the relevant indexes were measured by ELISA: tumor necrosis factor-α (TNF-α), interleukin-1β (IL-1β), procollagen amino-terminal peptide (type I procollagen amino-terminal peptide (P1NP)), type I collagen Carboxy-Terminal Peptide (CTX), VEGFA, endothelial inhibitor (endostatin) and VEGFA.

Statistical analysis:

Statistical analysis was performed using Excel 2013 (Microsoft Office Professional Plus 2013) and Statistical Package for the Social Sciences (SPSS) 26.0 (SPSS Inc., Chicago, IL). Normal distribution was expressed using the mean±standard deviation ($\bar{x}\pm s$). Independent-samples t tests were used to compare % DHI between the 2 modes of administration at each time point. Paired-samples t tests were used to analyze the significance of differences in % DHI between subgroups at different time points. One-way Analysis of Variance (ANOVA) was used to compare more than 3 groups when the data of multiple comparisons met the normal distribution and homogeneity of variance, and the Tukey test was used to compare the two groups; the Kruskal-Wallis test was used to compare the groups when the data did not meet the normal distribution or the homogeneity of variance and the hierarchical data. $p<0.05$ indicated that the differences were statistically significant.

TABLE 1: DIS GRADE WAS SCORED BLINDLY ACCORDING TO THE FOLLOWING CATEGORIES

Category	Score of 1 (normal)	Score of 5 (degenerative)
Annulus fibrosus grade	Normal pattern of fibrocartilage lamellae without ruptured fibers and without a serpentine appearance	Moderate/severe interruption
Border between the annulus fibrosus and the nucleus pulposus grade	Normal	Moderate/severe interruption
Cellularity of the nucleus pulposus grade	Normal cellularity	Moderate/severe decrease in the number of cells
Matrix of the nucleus pulposus	Normal gelatinous appearance	Moderate/severe condensation of the matrix
Endplate grade	Normal continuous and undisrupted	Complete disruption
Growth plate grade	Normal continuous and undisrupted	Complete disruption
Disc height grade	Normal disc height	Complete collapse
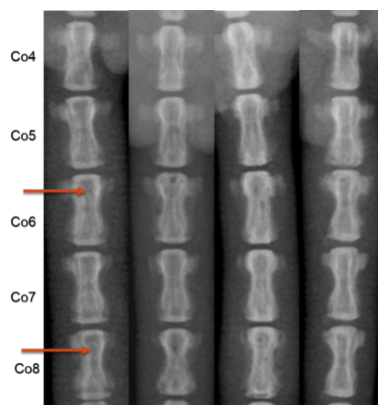
Fig. 1: X-ray of subchondral ossification in rats

RESULTS AND DISCUSSION

The DHI % measure had the smallest intra-observer error (SW value of 0.039370; % CV of 4.65 %) and inter-observer SW value of 0.042720 and % CV of 5.17 %. Cohen-kappa statistics were used to determine the intra and inter-observer reproducibility of the Pfirrmann grading scores and IDD histologic grading criteria scores of the sample MRIs. The Kappa values for intra- and inter-observer consistency for the Pfirrmann scores were 0.83 and 0.80, respectively; the intra- and inter-observer for IDD histologic scoring Kappa values for consistency were 0.82 and 0.76 for the IDD histologic score, indicating better consistency.

Relative to the blank group, the experimental group showed a decrease in intervertebral space height in the Co5/Co6 segment after 8 w of modeling, and subchondral osteosclerosis was observed in some rats (fig. 2). Over time, there was no statistically significant difference in the intervertebral space height changes in the Co7/Co8 segments. Meanwhile, unlike the Co7/Co8 segments, the DHI % of the Co5/Co6 segments was significantly and statistically different from that of the blank group (fig. 3).

The following manifestations could be observed from the MRI images; signal changes in the Co5/Co6 intervertebral space changed significantly with time extension. The height of the intervertebral space decreased and the Co5/Co6 IVD T2WI showed significant low-signal changes, suggesting that the IDD increased over time (fig. 4). According to the Pfirrmann grading, most of them were 1-2 grades at 2 w, most of them were 2-3 grades at 4 w, most of them were 3-4 grades at 8 w, and 5 grades of degeneration were seen in a few samples. And Co7/Co8 intervertebral MRI T2WI showed no significant change in signal compared with the blank control group.
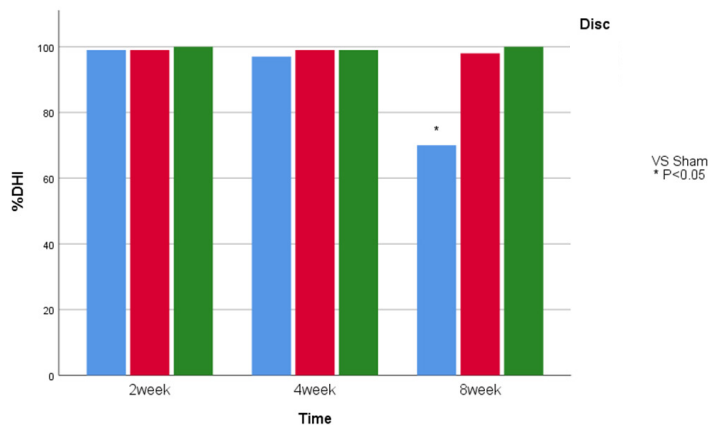
Fig. 2: Comparison of DHI % of rats in each group
Note: (■): Co5/6; (■): Co7/8 and (■): Sham
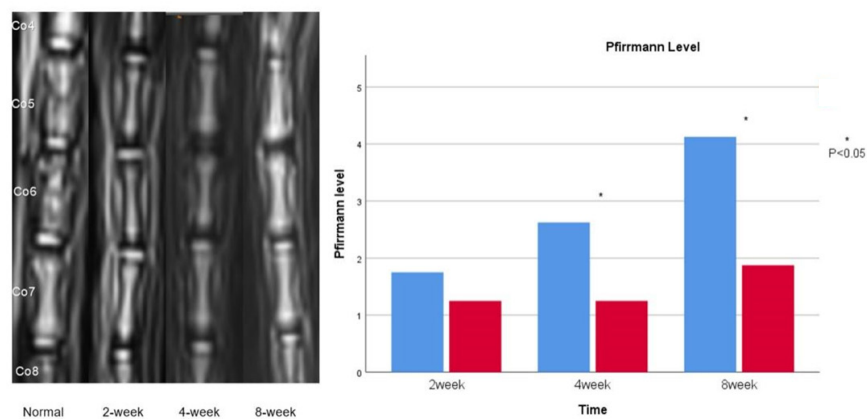
Fig. 3: Comparison of MRI imaging and IVD Pfirrmann grades in rats of each group
Note: (■): Co5/6 and (■): Co7/8
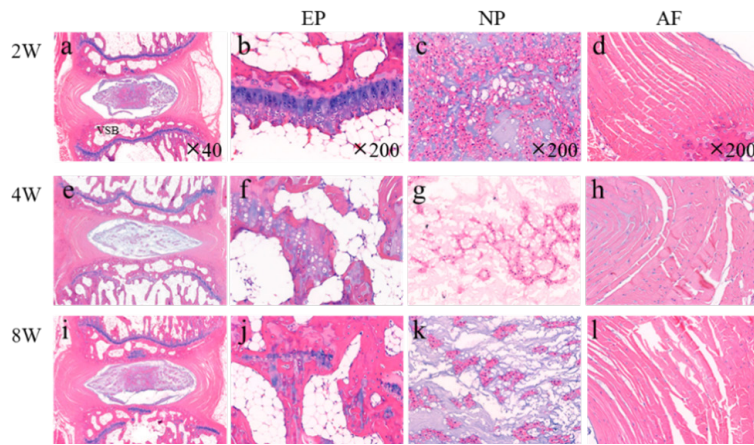
Fig. 4: EP: relative to at 2 w, (a and b): At the 8 w time period; (c and d): The VSB area showed a more pronounced reversal of osteoporosis (4 w slices to be adjusted), whereas the Growth Plate (GP) became thinner, and the end-plate structure broke down; (e-h): NP: a gradual increase in the number of vacuolated cells, which converted to chondrocytes and (i-l): AF: The concentric circle-like arrangement structure gradually thinned out and fissures appear

In the subchondral cancellous bone region at 2 w after modeling, the Tb. BMD, BV/TV, and Tb.Th of the upper endplate of Co6 were significantly lower than those of the blank group and the Co7/Co8 segment group (p<0.05), while in contrast, the Tb.Sp was significantly increased compared with that of the blank group and the Co7/Co8 segment group (p<0.05). In the subchondral bone plate region, Ct.Th and Ct.BMD values were significantly decreased in the Co6 upper endplate compared with the blank group and the Co7/Co8 segment group (both p<0.05). Overall, the Co6 upper endplates showed significant osteoporotic changes, while the Co8 upper endplate parameters did not show significant differences compared to the blank group.

When compared with the blank group and the Co7/Co8 segment group at 8 w after modeling, the Tb.BV/TV, Tb.Th were significantly increased in the subchondral cancellous bone region in the Co6 upper endplate, while Tb.Sp was significantly decreased (all p<0.05). Although the Tb.BMD index did not show significant differences compared with the other two groups, the index was significantly higher relative to that at 2 w. It suggests that the osteoporotic changes in this region were reversed and there was a sclerotic manifestation in the VSB region. In the subchondral bone plate region, compared with the blank group and the Co7/Co8 segment group, the Ct.Th and Ct.BMD of the upper endplate of Co6 still showed a decrease (p<0.05), suggesting that osteoporotic lesions still persisted in this region, but both indexes were significantly higher relative to those at 2 w, and there was no

significant difference in the changes of the indexes of the upper endplate of Co8 compared with those of the blank group (Table 2).

After imaging was completed, the animals were euthanized by an overdose of anesthetic. The Co5/Co6 and Co7/Co8 segments (each containing intact adjacent vertebrae on both sides and the IVD) were completely exfoliated. Sagittal noncontiguous 3 sections were cut from each of these specimens. The histologic presentation of IDD in each group of specimens (fig. 5 and fig. 6) showed that the VSB region showed osteoporotic changes at the early stage of modeling, and the osteoporotic state had been reversed at 8 w. The Growth Plate (GP) became progressively thinner and structurally broken after modeling, and there was a gradual increase in vacuolated cells in the NP (c,g,k). In contrast, the normal concentric circle-like structure of AF gradually thinned out and fissures appeared (d,h,l), and the degeneration of AF was relatively mild in 8 w compared with that of NP and VSB areas. Senna solid green staining showed degeneration and partial ossification of the growth plate cartilage with some disruption of the normal morphology. Similarly, a pale blue-stained cartilage matrix to bone matrix was seen in toluidine blue staining. From the histologic scores of the groups at different time periods (fig. 7), it was observed that at w 8, the histologic scores of the Co5/6 group were significantly higher than those of the Co7/8 group and the blank group; whereas, there was no statistically significant difference in the comparison between the Co7/8 group and the blank group (Table 3).

TABLE 2: MICRO CT DATA OF VERTEBRAL SUBCHONDRAL BONE AT 2 W

	Blank group	Co5/Co6 segment	Co7/Co8 segment
Trabecular region			
Tb. BMD (mg/cm^3)	366.10±31.22	248.35±22.58[ab]	321.19±32.55
Tb. BV/TV (%)	36.25±3.39	24.48±2.54[ab]	31.54±4.21
Tb. Th (μm)	114.85±32.58	74.39±21.05[ab]	115.81±0.28.33
Tb.N (cm^3)	3.18±0.45	2.49±0.24	2.73±0.33
Tb.Sp (μm)	238.93±27.63	396.69±42.72[ab]	237.93±18.30
Cortical region			
Ct.Th (μm)	283.25±35.64	197.34±42.18[ab]	295.44±25.64
Ct.BMD (mg/cm^3)	384.90±50.30	337.59±39.45[ab]	392.88±62.18

Note: abp<0.05, when compared with the blank group and the Co7/Co8 segment group by ANOVA, respectively and the difference was statistically significant
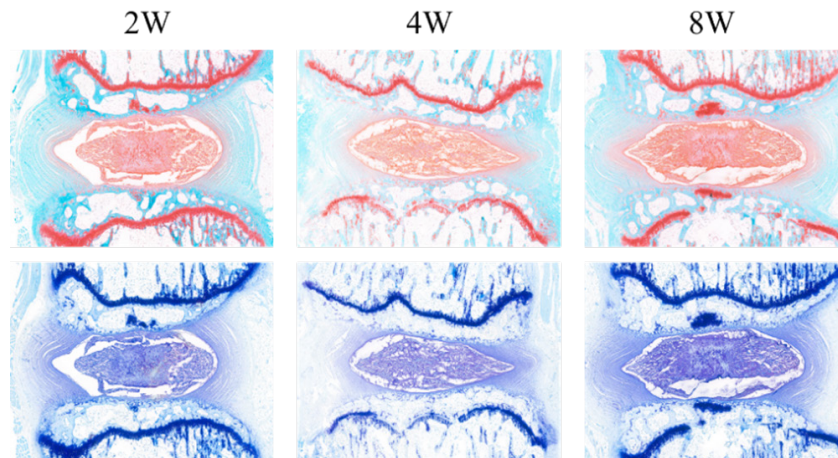
Fig. 5: Senna solid green staining (upper) shows that the red-stained GP located at the edge of the end plate gradually changed to light green, suggesting local cartilage degeneration and partial ossification until the local loss of normal morphology at 8 w. Toluidine blue staining (lower) suggests a shift from pale blue-stained cartilage matrix to bone matrix
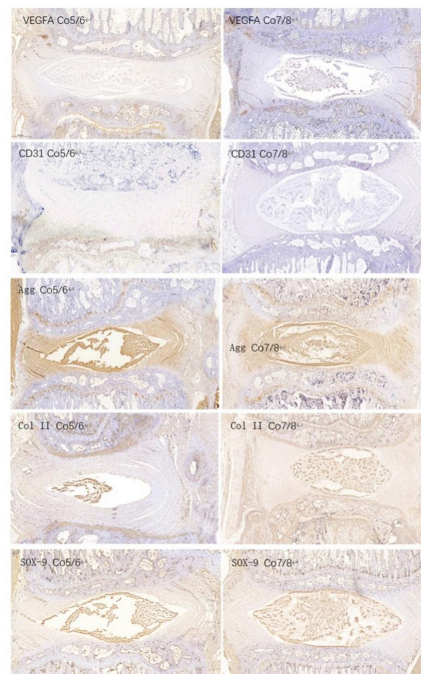
Fig. 6: Typical immunohistochemical staining showing differences in protein expression in Co5/6 and Co7/8 segmental IVD tissues
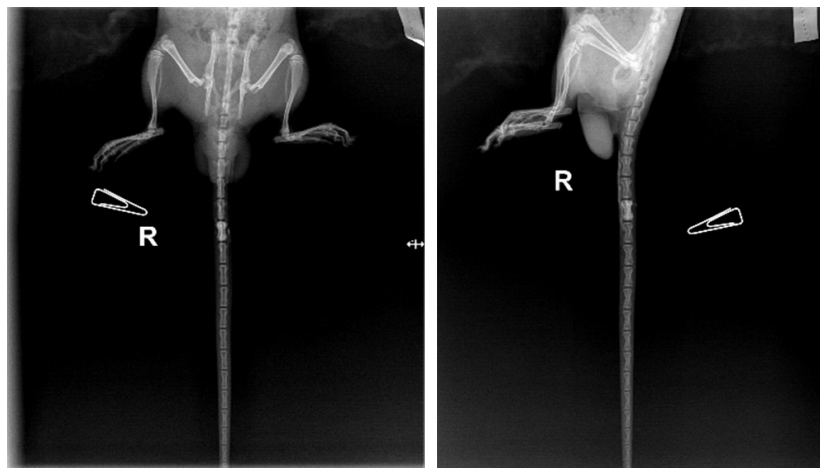
Fig. 7: In the pre-experiment, the illustrated high-density shadowed caudal vertebrae were taken after we added a small amount of iodixanol contrast agent to the AE, and it was still found that diffuse manifestations of the contrast agent were visible throughout the entire vertebral body of each rat

TABLE 3: MICRO CT DATA OF VERTEBRAL SUBCHONDRAL BONE AT 8 W

	Blank group	Co5/Co6 segment	Co7/Co8 segment
Trabecular region			
Tb. BMD (mg/cm^3)	368.45±1.42	370.51±3.44	367.48±3.15
Tb. BV/TV (%)	34.59±1.56	42.12±1.99[ab]	35.73±3.88
Tb. Th (µm)	117.15±4.31	137.16±3.46[ab]	118.54±4.24
Tb.N (cm^3)	3.63±0.80	3.81±0.18	3.77±0.27
Tb.Sp (µm)	282.18±12.44	254.50±8.46[ab]	277.50±9.45
Cortical region			
Ct.Th (µm)	303.71±8.18	276.81±15.71[ab]	299.35±13.14
Ct.BMD (mg/cm^3)	387.09±21.36	357.59±39.45[ab]	390.02±20.92

Note: [ab]$p<0.05$, when compared with the blank group and the Co7/Co8 segment group by ANOVA, respectively and the difference was statistically significant

At the 2 w time point, VEGFA immunohistochemically positive staining was significantly higher in the ischemic side of the endplates of the Co5/6 segment group (Co6 upper endplates) than in the normal side (Co5 lower endplates) as well as in the control Co7/Co8 segments. There was a trend of decreasing positive staining for Col II and aggrecan in the NP. SOX-9 is present in the NP and is a key gene in cartilage and in the development and differentiation of Col II. Similarly, SOX-9 protein levels in the NP of the Co5/6 segment group gradually decreased with time progression (fig. 8). The above typical protein expression further corroborates the IDD in Co5/6 segment.

The serum levels of CTX in the modeling group of rats were significantly higher at 2 w compared to the blank group, while the levels of P1NP were significantly lower at 2 w and significantly higher at 8 w relative to the blank group (both p<0.05) (fig. 9 and fig. 10).

The expression of TNF-α and IL-1β associated with inflammation was significantly higher than that of the blank group at both 2 w and 8 w (p<0.05) (fig. 11 and fig. 12).

Compared with the blank group, the content of VEGFA and endostatin, which are associated with neoangiogenesis, was significantly higher at 2 w (p<0.05), and their expression was not significantly different from that of the blank group at 8 w (p<0.05) (fig. 13 and fig. 14).

Previous understanding of the pathology and physiology of the IVD has focused on the medulla as well as the annulus fibrosis. In recent years, more scholars have recognized the endplates as another important component of the IVD. The vertebral endplates are structurally and functionally categorized into Cartilaginous Endplates (CEPs)

and Bony Endplates (BEPs) - i.e., subchondral bone, VSB.

Given the special anatomical characteristics of the IVD and the dependence of the body on the IVD for various life activities, the IVD is susceptible to degeneration. Previous studies have suggested that the main causes of disc degeneration include hypoxic-ischemic state due to impaired nutrient transport, interference by inflammatory factors, immune response, abnormal loading, and genetic factors.

VSB is a general term for the cortical and trabecular layer of bone with vascularized tips between the cartilaginous endplate and the vertebral body. It is connected to the IVD through the cartilaginous endplate and plays an important role in maintaining the normal physiologic function of the spine and the IVD. First, it provides a good stress cushion for other tissues of the IVD between the IVD and bone, which have very different densities and strengths, and ensures the integrity of the cartilaginous endplate. Second, the subchondral bone strongly counteracts the hydrostatic pressure on the medullary nucleus of the IVD, preventing the nucleus from protruding in an upward and downward direction and causing Schmoe's nodes. Third, the subchondral bone is the guarantee of the nutritional supply of the IVD. Adult IVD is an immune-exempt tissue with no blood supply, and its nutrient transport mainly relies on the diffusion and penetration of the vascular-rich subchondral bone.
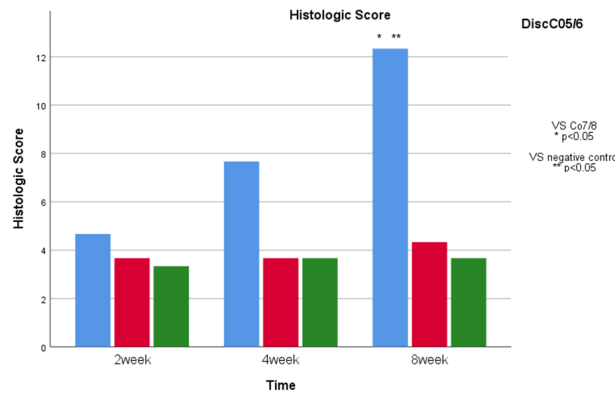
Fig. 8: Difference in IVD histological scores between groups at different time points
Note: (■): Co 5/6; (■): Co7/8 and (■): Negative control
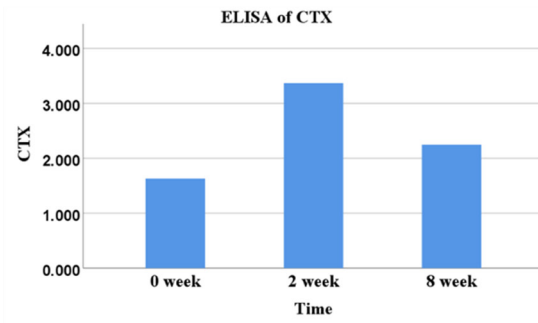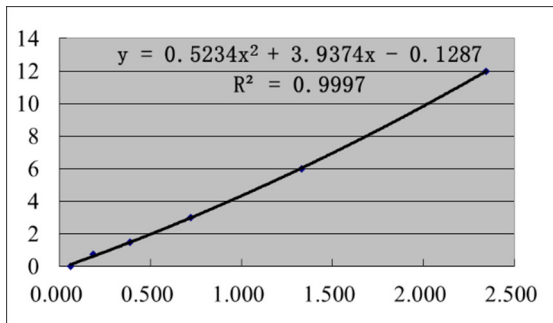
Fig. 9: Comparison of CTX standard curve and concentration
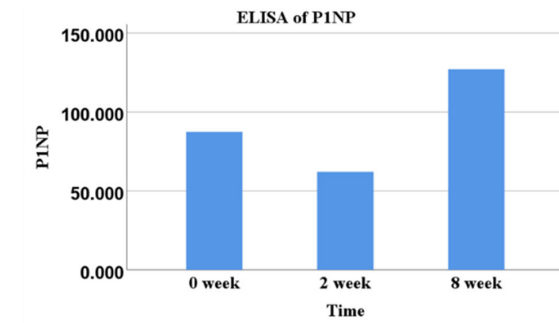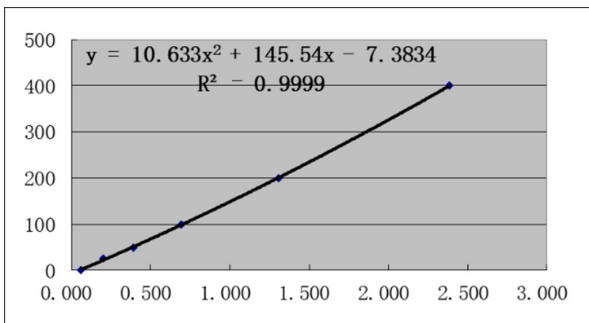
Fig. 10: Comparison of P1NP standard curve and concentration

$$y = 48.295x^2 + 361.96x - 32.038$$
$$R^2 = 0.9989$$
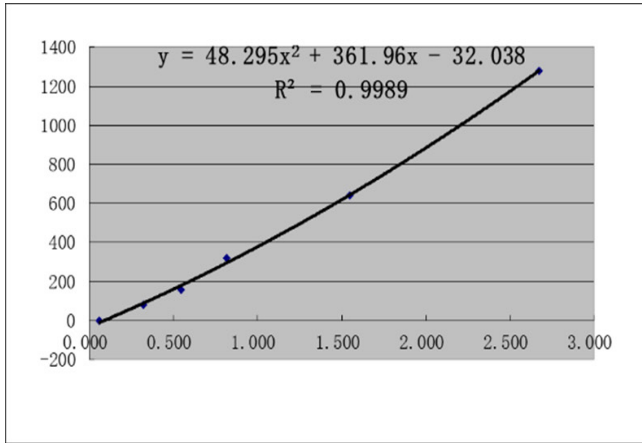
Fig. 11: VEGFA standard curve and concentration comparison

$$y = 165.04x^2 + 269.82x + 10.81$$
$$R^2 = 0.9986$$
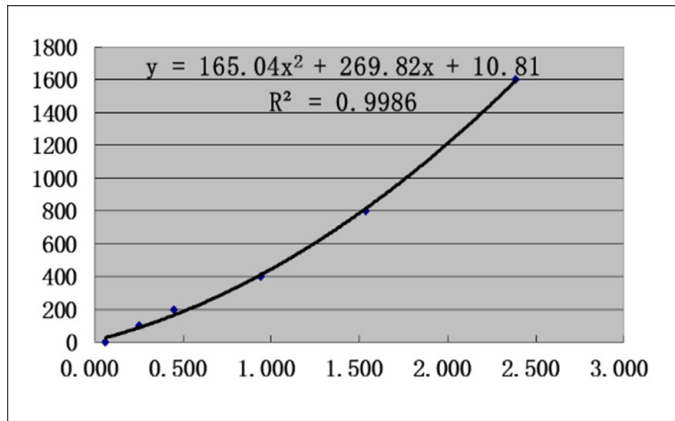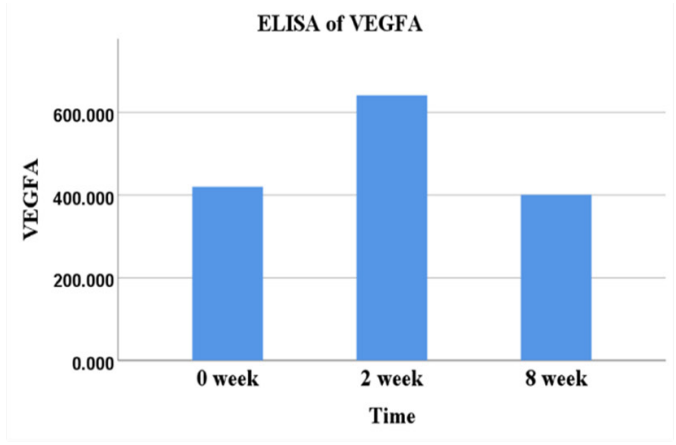
Fig. 12: Comparison of endostain standard curve and concentration

$$y = 50.367x^2 + 67.116x + 0.24$$
$$R^2 = 0.9995$$

Fig. 13: Comparison of TNF-α standard curve and concentration

$$y = 0.9949x^2 + 2.5477x + 0.0138$$
$$R^2 = 0.998$$
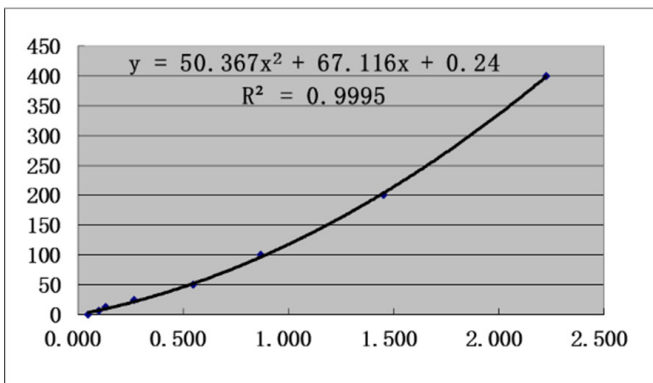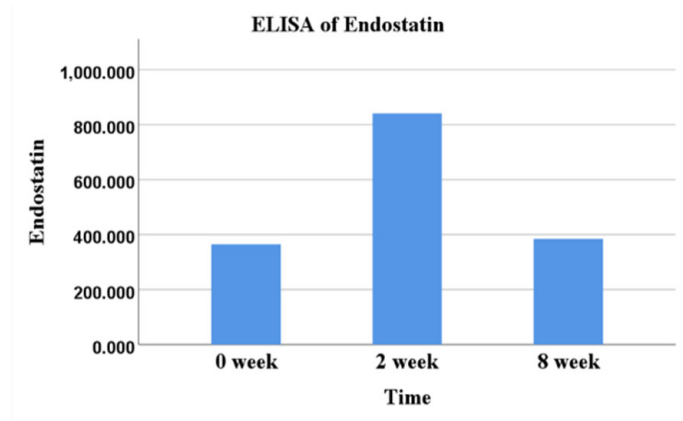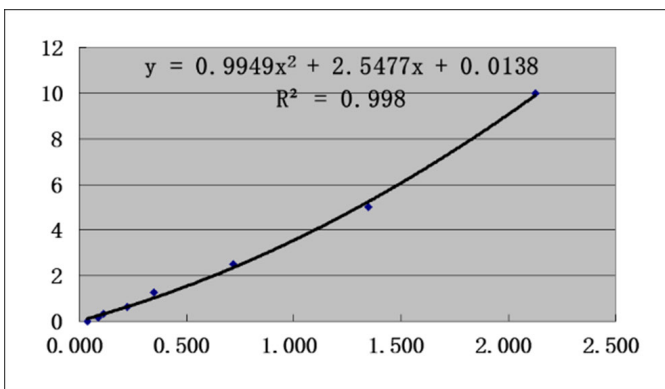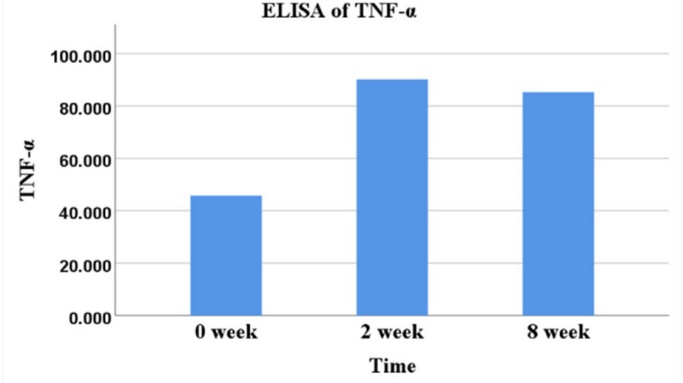
Fig. 14: Comparison of IL-1β standard curve and concentration
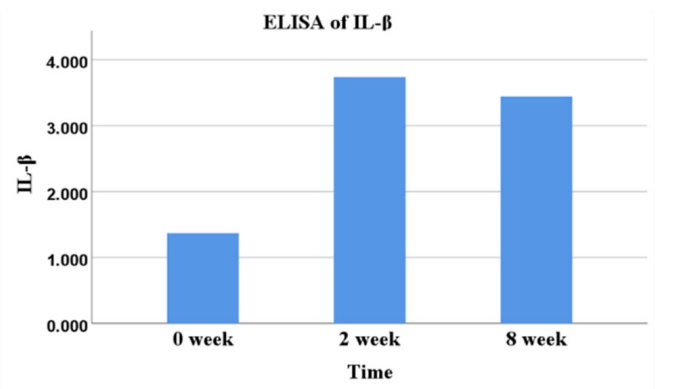
More and more studies suggest that the VSB, as the most important nutrient transport pathway of the intervertebral disc, is closely related to IDD, and that the early stage of VSB lesions can affect the process of IDD. microstructural changes in the VSB lead to the initiation of bone remodeling programs, and the abnormal and imbalanced activity of osteoblasts and osteoclasts gradually lead to the sclerosis of the VSB, which results in a reduction of the permeability of the vessels in the VSB, and a reduction in the buffering capacity of the VSB to protect the IVD effectively, thereby exacerbating the problem of the IVD. It is difficult to protect IVD effectively, thus exacerbating the IDD process.

Thus, the study of VSB in the process of IDD is of great significance. However, no systematic description of VSB in the early stage of IDD has been presented. For this reason, the present study used sub endplate anhydrous alcohol injection as an initiating factor in the IDD model of SD rats, in an attempt to verify the evidence that VSB lesions can be used as an initiating factor for IDD and to explore the characteristics of VSB lesions in this model.

This model was slightly adapted from the one reported by Yuan *et al*.[1]. First, in the pre-experiment, we observed the diffusion and leakage of AE by dropping a little methylene blue into AE as a stain. Too much dose of AE and too fast injection are easy to lead to leakage, and finally we took the dose and injection speed and way similar to that reported by Yuan *et al*: The dose

was 30 µl for each segment, and we pushed the injection slowly with a 1 ml specification syringe containing 0.6 ml of air until after tens of seconds, the pressure in the syringe gradually weakened and disappeared on its own, indicating that the drug was completely injected under the endplate. Interestingly, however, we found that despite strict control of the dose, injection speed and pressure of AE injection, the diffusion of AE in the tailbone of SD rats tended to fill the entire cancellous bone region of the vertebrae. Therefore, in order to visualize the diffusion, we added a small amount of iodixanol (contrast agent) to the AE and performed X-ray examinations of the tailbone of SD rats immediately after the routine injection of AE, and we still found that the diffusion of the contrast agent was seen throughout the entire vertebral body of each rat (fig. 15). The above manifestations led us to think that the puncture injection below the upper endplate might affect the VSB blood supply of the lower endplate of this vertebra, thus interfering with the neighboring distal IVD manifestations. The Co4/Co5 segment overlaps with the rat scrotum in the anterior-posterior direction, and in the prone position, this segment is a region of excessive migration, which makes it difficult to lie flat on the tabletop, which is unfavorable for puncture and imaging; this is similar to the findings of previous scholar[3]. Therefore, we changed the puncture segments from Co7/Co8 and Co8/Co9 segments to Co5/Co6 and Co7/Co8 segments. The proximal larger vertebrae also facilitated the experimental operation and improved the consistency of the operation.
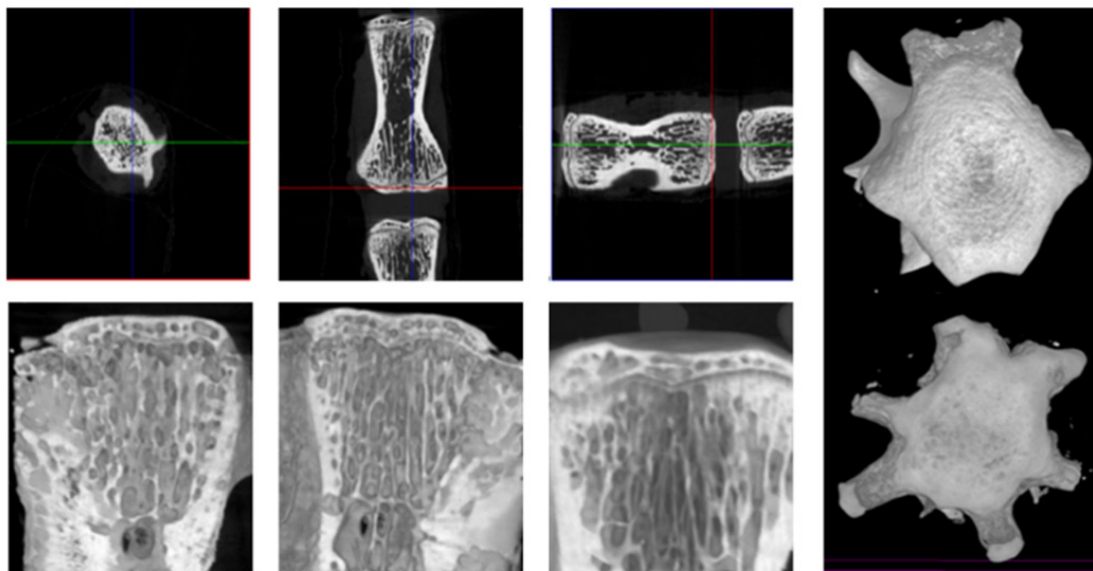
Fig. 15: Typical micro CT image

The results of this experiment found that due to the destruction of vascular tissues in the VSB region by anhydrous alcohol, Co5/Co6 segments gradually showed typical IDD manifestations at the levels of imaging, histomorphometry and immunohistochemically analysis over time after modeling. X-ray showed reduction of the vertebral space, sclerosis of the endplates, and bone redundancy formation, etc.; the T2 image of MRI showed gradual diminution of the IVD signals, the T2 image of MRI showed a gradual weakening of the IVD signal, and the Pfirrmann grading was higher compared with that of the control group, with statistically significant differences; HE staining, saffron solid green staining and toluidine blue staining clearly showed the degeneration of the IVD nucleus pulposus, annulus fibrosis, and endplates. Comparatively speaking, AF degeneration within 8 w was mild, which is similar to the results reported in the past[1], one of the reasons may be that normal AF tissues do not have blood supply, and the present ischemic model has less direct effect on its early stage; another may be that the AF structures were not directly damaged in the present model, relative to the other AF puncture IDD models. We will observe the AF for a longer period of time in the next experimental program. In addition, immunohistochemically analysis provided localization analysis of proteins specific to different tissue components of the IVD, and the experimental results likewise corroborated the IDD of the modeled segments. In summary, our results were similar to human IDD and previous animal experiments reported in the literature, and the animal model showed satisfactory stability and consistency through refinement of experimental details.

While verifying the success of modeling, we focused on the multidimensional pathological features of IDD segmental VSB. At the imaging level, we observed the gradual sclerosis of the VSB by X-ray, and these changes could even be demonstrated in T2 like MRI imaging. microCT provided us with a better perspective to observe the VSB through the image observation and data analysis of this examination, we obtained a more fine-grained process of bone remodeling and characteristics of the VSB region in the early stage of IDD. At the early stage of the molding process, due to the relatively active function of the osteoclasts, the VSB region is more sensitive to

bone remodeling. At the early stage of modeling, due to the relatively active function of osteoclasts, the VSB region first showed a decrease in bone mass, followed by an increase in VSB bone density and bone volume. The abnormal bone remodeling led to the sclerosis of the VSB, which may be the main cause of the impaired nutrient transport in the IVD and the cause of IDD. And at the histologic level, we observed a gradual decrease in chondrocyte staining, which was gradually and partially replaced by calcified tissue. In addition, immunohistochemistry showed that VEGFA staining in the VSB region of Co5/Co6 segments was significantly less than that of control Co7/Co8 segments, further confirming the destructive effect of AE on blood vessels. At the serological level, the CTX content in the serum of rats in the modeling group was significantly increased at 2 w, and the P1NP content was first decreased and then increased, suggesting that abnormal bone remodeling in which osteoblastic and osteogenic activities successively predominated in the VSB region occurred. At 2 w after modeling, TNF-α, IL-1β, VEGFA, and endostatin were significantly elevated, suggesting that the VSB had an active local inflammatory response and vascular destruction at an early stage, and the levels of VEGFA and endostatin decreased to the level of the blank group at 8 w, suggesting that the early elevation of these two substances was probably due to the transient vascular destruction and inflammatory response induced by the injection of anhydrous alcohol into the local VSB disruption and inflammatory response. This is in general agreement with the report of Li et al.[6]. It does not mean that mature neovascularization in the VSB region improves the trophic pathway of the IVD, because histological staining of the endplates at different time points did not reveal that the central region of the VSB in the Co5/6 segments (Co6 upper endplates) had a greater number of blood vessels than those in the Co7/8 segments.

Previous studies seem to be unclear about the causal relationship between early IDD and VSB. Nguyen et al.[7] concluded that VSB is critical for spinal function. With age aging or injury, lesions of the VSB may lead to spinal dysfunction, IDD and nonspecific lower back pain. Rutges et al.[8] applied microCT measurements of cadaveric IVD specimens and found that compared to intact IVD, VSB in mildly degenerated IVD had higher bone

volume and trabecular thickness, suggesting that VSB changes are closely related to early IDD. Ziran *et al.*[9] found that imaging and histologic changes in the VSB of gerbils, a model of spontaneous IDD, were observed before IDD and contributed to the acceleration of IDD. Whereas it is well known that lesions in the VSB at the time of IDD can often be observed both in the clinic and in the laboratory, especially the many IDD models that act only on the nucleus pulposus and the annulus fibrosus have been repeatedly validated and routinely applied[10-12]. Therefore, it is more likely that there is a complex interaction between the two, which influence each other and are causal at different stages of the lesion.

In the author's experiments, AE was simply acted under VSB without direct contact with other IVD components (NP, AF, CEP), and the experimental results suggested that this method successfully induced IDD. This strongly suggests that IDD can be caused by VSB lesions, and considering that the experimental animals can be regarded as free of other factors such as age-related degeneration and trauma before modeling, VSB may be the initiator of IDD in the present experimental animals, as well as some clinical IDD. VSB may be the initiating factor of IDD in the present experimental animals as well as some IDD in the clinic. And this is consistent with the view of Wang *et al.*[13] and other scholars.

The first comprehensive investigation of the lesion characteristics of VSB in the early stage of IDD degeneration model, which provides the basis for the subsequent exploration of the mechanism and provides reference for other researchers.

Overall, on the basis of previous IDD animal models, this study successfully established an IDD animal model mediated by the IVD nutrient pathway disorder in the VSB region by fine-tuning the modeling method. And for the first time, the lesion characteristics of VSB in the rat caudal vertebrae IDD model were characterized in a more systematic way, which can provide a possible reference for the subsequent research on the etiology of IDD related to VSB and drug therapy. The present study also has the following shortcomings; first, given the differences in structure and biomechanics between the IVDs of SD rats and humans, the results of this study cannot be directly applied to the clinic for the time being.

Second, the specific mechanism of IDD caused by VSB lesions is still not completely clear. Abnormal bone remodeling in the VSB region, occlusion of vascular pathways, and inflammation may be the main factors in this model, and the interactions among these three factors and their interactions need to be investigated in further molecular biology studies. Finally, considering that previous studies have suggested that drug interventions are ineffective in the late stage of IDD, only the early stage of IDD VSB lesions were observed in the model animals in this study, and the observation period will be extended in subsequent studies to understand the characteristics of the VSB lesions in the whole stage of IDD, so as to provide more complete data support for the subsequent drug interventions.

Authors' contribution:

Hao Qu and Feng Wang have contributed same to this work

Conflict of interests:

The authors declared no conflict of interests.

REFERENCES

1. Yuan W, Che W, Jiang YQ, Yuan FL, Wang HR, Zheng GL, *et al.* Establishment of intervertebral disc degeneration model induced by ischemic sub-endplate in rat tail. Spine J 2015;15(5):1050-9.

2. Kim KS, Yoon ST, Li J, Park JS, Hutton WC. Disc degeneration in the rabbit: A biochemical and radiological comparison between four disc injury models. Spine 2005;30(1):33-7.

3. Han B, Zhu K, Li FC, Xiao YX, Feng J, Shi ZL, *et al.* A simple disc degeneration model induced by percutaneous needle puncture in the rat tail. Spine 2008;33(18):1925-34.

4. Pfirrmann CW, Metzdorf A, Zanetti M, Hodler J, Boos N. Magnetic resonance classification of lumbar intervertebral disc degeneration. Spine 2001;26(17):1873-8.

5. Allon AA, Aurouer N, Yoo BB, Liebenberg EC, Buser Z, Lotz JC. Structured coculture of stem cells and disc cells prevent disc degeneration in a rat model. Spine J 2010;10(12):1089-97.

6. Li XF, Xue CC, Zhao YJ, Cheng SD, Zhao DF, Liang QQ, *et al.* Deletion of Opg leads to increased neovascularization and expression of inflammatory cytokines in the lumbar intervertebral disc of mice. Spine 2017;42(1):E8-14.

7. Nguyen C, Poiraudeau S, Rannou F. Vertebral subchondral bone. Osteoporos Int 2012;23(S8):857-60.

8. Rutges JP, Oner FC, Verbout AJ, Castelein RJ, Kummer JA,

Weinans H, *et al.* micro-CT quantification of subchondral endplate changes in intervertebral disc degeneration. Osteoarthr Cartil 2011;19(1):89-95.

9. Ziran BH, Pineda S, Pokharna H, Esteki A, Mansour JM, Moskowitz RW. Biomechanical, radiologic and histopathologic correlations in the pathogenesis of experimental intervertebral disc disease. Spine 1994;19(19):2159-63.

10. Elmounedi N, Bahloul W, Turki M, Amri R, Aoui M, Elbaya W, *et al.* Impact of needle size on the onset and the progression of disc degeneration in rats. Pain Physician 2022;25(6):509.

11. Tam V, Chan WC, Leung VY, Cheah KS, Cheung KM, Sakai D, *et al.* Histological and reference system for the analysis of mouse intervertebral disc. J Orthopaedic Res 2018;36(1):233-43.

12. Masuda K, Aota Y, Muehleman C, Imai Y, Okuma M, Thonar EJ, *et al.* A novel rabbit model of mild, reproducible disc degeneration by an anulus needle puncture: Correlation between the degree of disc injury and radiological and histological appearances of disc degeneration. Spine 2005;30(1):5-14.

13. Wang P, Zhou Z, Zhang H, Tian F, Wang W, Zhang L. Vertebral subchondral bone and intervertebral disc degeneration. Zhongguo Xiu Fu Chong Jian Wai Ke Za Zhi 2015;29(3):377-80.